Detecting water ingress in aviation honeycomb panels: qualitative and quantitative aspects

Vladimir Vavilov[a,b], Sergio Marinetti[c], Yangyang Pan[a], Arsenii Chulkov[a]

[a] Tomsk Polytechnic University, Lenin Av., 30, Tomsk 634050, Russia
[b] Tomsk State University, Lenin Av., 36, Tomsk 634050, Russia
[c] Istituto per le Tecnologie della Costruzione- Consiglio Nazionale delle Ricerche, Corso Stati Uniti, 4, Padua, Italy

Abstract

We have used infrared tomography to study water trapped in aviation honeycomb panels, namely: 1) possibility of quantitative evaluation of trapped water, 2) influence of honeycomb panel orientation on the efficiency of water detection, and 3) discrimination between honeycomb cells filled with water and adhesive. It is shown, both theoretically and experimentally, that it is difficult to discriminate between water and epoxy adhesive by analyzing only surface temperature patterns. The concept of apparent effusivity has demonstrated that water trapped in a cell can be reliably detected by an increase in effusivity starting from the inflection time.

Keywords: active thermal nondestructive testing, honeycomb structure, water ingress, effusivity evaluation

1. Introduction

Honeycomb reinforced composite panels are widely used in aircraft structures, such as ailerons, flaps, keels, rudders, etc. They are sturdy and lightweight but they are susceptible to ingress of water from the atmosphere. At high altitude, any water trapped in honeycomb cells can freeze and expand, and this may cause damage to the honeycomb cells or to the structure itself. Testing for trapped water is typically done by a time-consuming contact ultrasonic point inspection technique. Ultrasonic nondestructive testing (NDT) is also widely used for inspecting damage in composites [1]. In the aerospace industry, the most typical technique for the inspection of large polymeric structures is ultrasonic C-scan, which either immerses the part in a water bath or squirts columns of water onto the part. Unfortunately, during this inspection process, water can get into the part by various mechanisms, including leakage, diffusion or

absorption. This trapped water must generally be removed before flight, and this is usually done by heating the part in an oven or autoclave. This drying process can add considerable cost and time to the processing of the part. And sometimes not all the water is removed.

Another popular technique for detecting trapped water in honeycombs is infrared (IR), or thermal, NDT (TNDT) [2]. Due to its high heat capacity (high thermal inertia), water changes temperature relatively slowly after being exposed to a transient thermal pulse, which may be either positive or negative.

Therefore, the corresponding temperature indications over hidden water are characterized by significant amplitudes and long survival times, thus facilitating their identification even by inexperienced operators. Some aspects of IR thermographic water detection have been discussed in [2-5], and the corresponding inspection practices involving active TNDT procedures are being used by Boeing and Airbus corporations [6, 7]. However, for evident reasons, earlier studies did not attempt to evaluate the mass of hidden water, and the corresponding quantitative estimates have been obtained by using ultrasonic testing. Another proposed technique exploits a significant temperature gradient that occurs between a cruising altitude and the ground level, therefore, trapped water can be reliably detected immediately after landing [3]. An example of detecting cell water in a Toupolev-204 fuselage at 45 minutes after landing is shown in Fig. 1 to illustrate a qualitative aspect of testing.

In this study, we address some novel aspects of IR thermographic water detection which are of practical interest, namely: 1) possibility of quantitative evaluation of trapped water, 2) influence of honeycomb panel orientation on the efficiency of water detection, and 3) discrimination between honeycomb cells filled with water and epoxy adhesive.

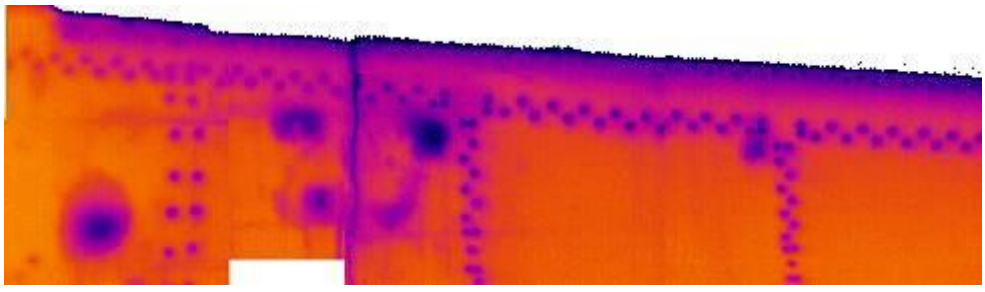

Fig. 1. IR thermogram of Toupolev-204 fuselage (45 minutes after landing, up to 6 hidden water sites are clearly seen with differential temperature signals from 5 to 9 ^{o}C).

2. Water detection models

Inspection cases analyzed in this study are presented in Fig. 2. The ideal inspection case is that when hidden water is in contact with a honeycomb skin to be tested (inspection direction ID #1 in Fig. 2). In this case, water can fully or partially fill honeycomb cells, and the challenging inspection task is to approximately evaluate water mass. If, because of gravity, water descends to the cell bottom, while the panel is to be tested from the top (ID #2), the presence of an air gap thermally insulates the water thus decreasing temperature signals. The third test case appears when water partially fills honeycomb cells but the inspection is fulfilled sideways (ID #3), as it appears when checking a rudder. In this case, the water is in contact with the skin but a 'lateral' defect size might be small for reliable detection. We call this situation 'side' or 'capillary' water because it also simulates a small amount of water distributed in a cell due to capillary forces. Another goal of TNDT is to discriminate between honeycomb cells filled with water or filled with an adhesive (called 'epoxy' below). Since adhesive is acceptable and water is not, the ability to reliably discriminate between these materials may prevent unnecessary and costly repair of aircraft panels.

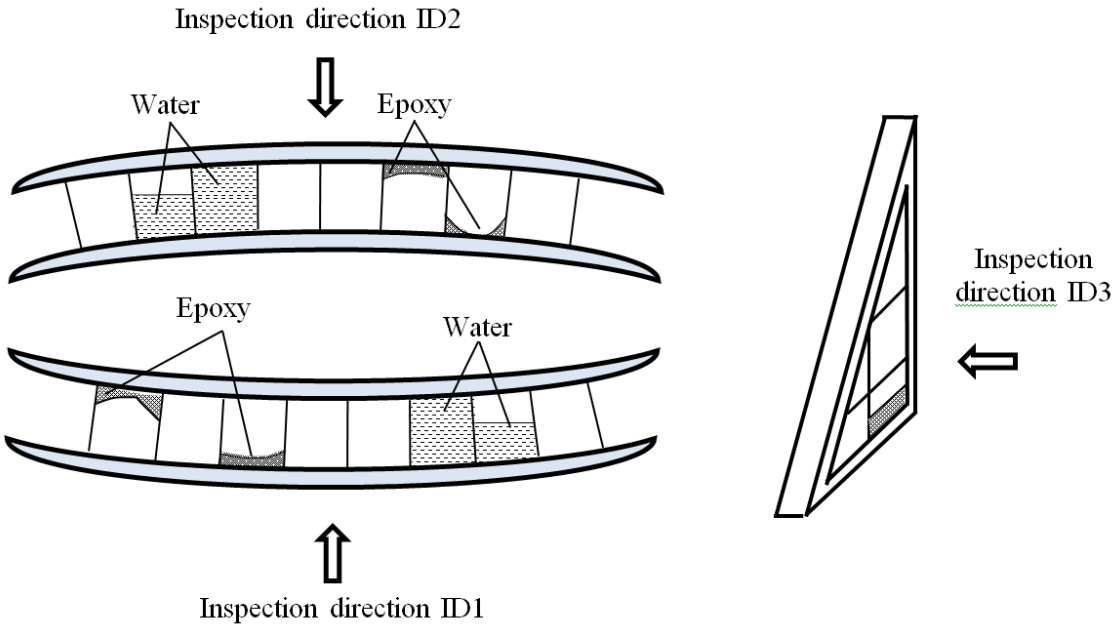

Fig. 2. Water ingress test cases.

The real test geometries presented in Fig. 2 are simulated with the three-dimensional (3D) Cartesian models shown in Fig. 3.

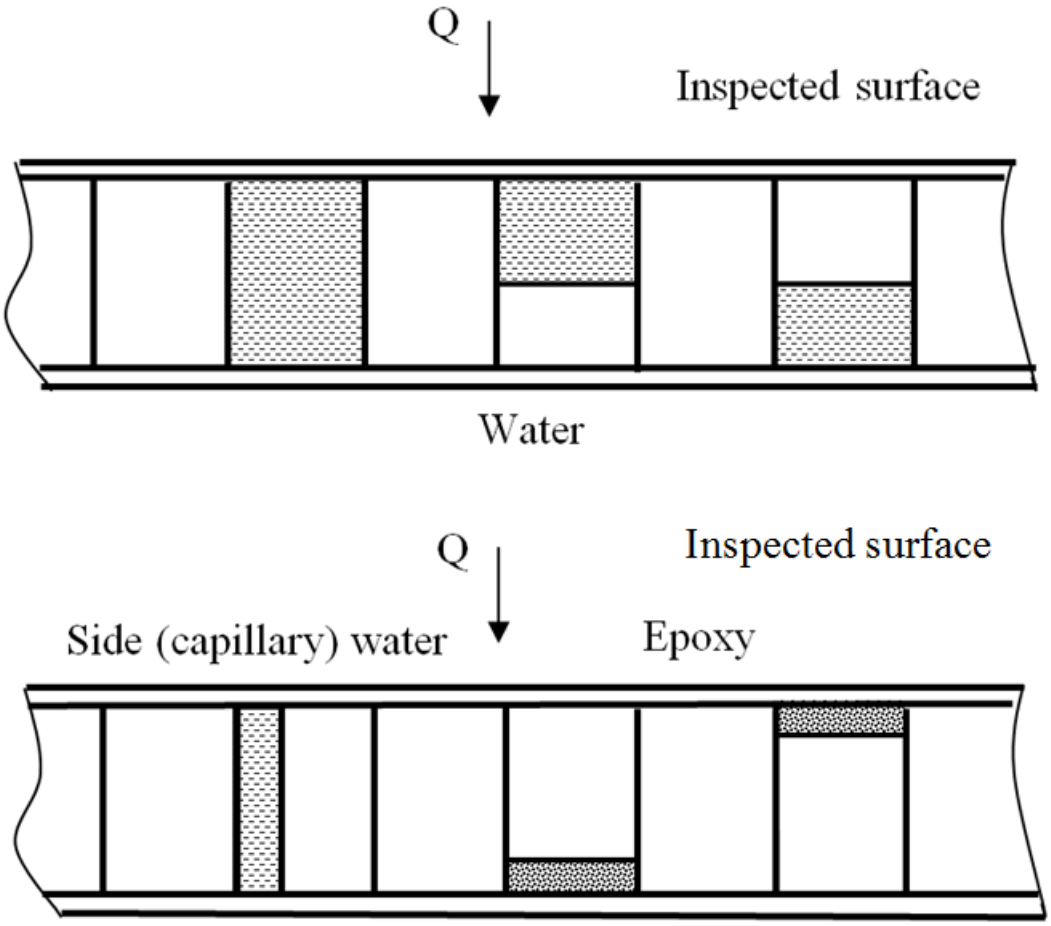

Fig. 3. Water ingress test models.

3. Analytical and numerical solutions

3.1. Test models

The models in Fig. 3 have been analyzed analytically and numerically. It is well known that, in most cases, analytical solutions describe temperature evolutions either in non-defect areas or in large-size defect areas where temperature distributions are can be considered one-dimensional (1D).

The following heat conduction solutions are widely used in TNDT.

Flash heating of an adiabatic semi-infinite body:

$$T_{SIB}(\tau) = \frac{W}{e\sqrt{\pi\tau}}. \quad (1)$$

Flash heating of an adiabatic plate:

$$T_P(\tau) = \frac{Wa}{\lambda L}\left[1 + 2\sum_{n=1}^{\infty} e^{-n^2\pi^2 Fo}\right]. \quad (2)$$

Flash heating of a coating on a semi-infinite substrate:

$$T_c(\tau) = \frac{Wa}{e_c\sqrt{\pi\tau}}\left[1 + 2\sum_{n=1}^{\infty}(-G)^n e^{-\frac{n^2}{Fo_c}}\right]. \quad (3)$$

Here: τ is the time, W is the absorbed energy, e is the thermal effusivity, a is the thermal diffusivity, λ is the thermal conductivity, L is the plate thickness, $Fo=a\tau/L^2$ is the Fourier number, $G=(e_s-e_c)/(e_s+e_c)$ is the thermal wave reflection coefficient, and "c" and "s" subscripts denote a coating and a substrate respectively.

More realistic water detection models analyzed by using ThermoCalc-3D (former ThermoCalc-36L, Tomsk Polytechnic University, Russia) software are shown in Fig. 4. This numerical software allows modeling up to 36 sample layers which may contain up to 40 parallelepiped-like defects. The models in Fig. 4 include 9 honeycomb cells (Fig. 4a) of which one is filled with water and another - with epoxy. The following defect situations have been analyzed: water/epoxy fills respectively 100, 50, 10 and 5 % of cell volume being in contact with the front or rear honeycomb skin (in Fig. 4 heating takes place from the bottom in all cases). The numerical grid has been 400×400×75, the heating has been performed with a flash (pulse duration 0.01 s, heating power 10^6 W/m^2, or 10^4 Jm^{-2} in terms of energy, calculation step 0.01 s). The primary purpose of this work was to evaluate the probability of detection of water that partially fills the honeycomb cells of a horizontal aircraft panel. Due to gravity, the water will be in contact with the lower surface and not in contact with the upper surface. Therefore, the inspection would be normally performed by applying heat to the lower surface while monitoring that surface with an IR camera. An academic question would be whether an inspection from the upper surface could detect water that is not in contact with the upper surface, and further, what level (percent cell height) of water can be detected. The second purpose of this work was to develop a TNDT technique that can discriminate between water and adhesive.

Material thermal properties used in calculations are presented in Table 1.

Table 1. Material thermal properties*

Material	Thermal conductivity λ, W/(m·K)	Heat capacity, C, J/(kg·°C)	Density ρ, kg/m^3	Thermal diffusivity a, m^2/s	Thermal effusivity e, W·s$^{1/2}$/(m^2·°C)
Carbon fiber reinforced plastic (CFRP)	0.61	1758	1500	$2.31 \cdot 10^{-7}$	1268
Glass fiber reinforced plastic (GFRP)	0.30	1775	1300	$1.30 \cdot 10^{-7}$	832.0
Water	0.59	4193	1000	$1.41 \cdot 10^{-7}$	1573
Epoxy	0.18	1100	1200	$1.36 \cdot 10^{-7}$	487.4
Air	0.07	928.4	1.3	$5.8 \cdot 10^{-5}$	9.192

* Reflection coefficient G for CFRP-air: -0.986, CFRP-water: 0.107,
CFRP-epoxy: -0.445;
GFRP-air: -0.978, GFRP-water: 0.308, GFRP-epoxy: -0.261.

3.2. Modeling results

3.2.1. Water/epoxy discrimination

Figure 4a shows 1D temperature histories over the non-defect honeycomb skin and the areas filled with water and epoxy calculated by Eq. (3). All three curves look similarly being characterized by different steady-state temperature values. We remind that, in the case of homogeneous plates, these values are equal to $Wa/\lambda L$, as follows from Eq. (2) in the absence of heat exchange with the ambient.

The lowest temperature rise occurs over water because of its high heat capacity. However, since the water mass and test conditions are not consistent, the discrimination between water and epoxy by analyzing only surface temperature will be difficult.

To solve this problem, we suggest using the concept of apparent thermal effusivity e_{ap} by inverting Eq. (1):

$$e_{ap}(\tau) = \frac{W}{T_{exp}(\tau)\sqrt{\pi\tau}}, \quad (4)$$

where $T_{\exp}(\tau)$ is the experimental temperature evolution, and the e_{ap} parameter is called apparent ('*ap*') effusivity. When processing experimental data, Eq. (4) is frequently used in the normalized form:

$$e_{ap}(\tau)/W = \frac{1}{T_{exp}(\tau)\sqrt{\pi\tau}}. \quad (5)$$

Analysis of e_{ap} becomes particularly fruitful in the case of layered samples, as shown in Fig. 5b. Immediately after flash heating and up to the inflection time τ_{inf}, apparent effusivity is equal to the effusivity of the first layer (skin) that is 1268 $W{\cdot}s^{1/2}/(m^{2.o}C)$ in the case of CFRP. Starting from τ_{inf}, apparent effusivity goes toward a value which corresponds to the second layer. In our case, over air-filled cells, e_{ap} drops down to about 9 $W{\cdot}s^{1/2}/(m^{2.o}C)$. Qualitatively, the same behavior is observed over cells filled with epoxy adhesive of which effusivity is lower than that of CFRP. Since the water is characterized by a higher effusivity than all other materials involved, e_{ap} grows up at $\tau > \tau_{inf}$ with the limit being equal to 1573 $W{\cdot}s^{1/2}/(m^{2.o}C)$. Hence, water sites can be reliably identified by simply analyzing the behavior of apparent effusivity at times longer than τ_{inf}.

The concept above has been also validated in the framework of the 3D water detection model from Fig. 4. In calculations, the heat time duration was 0.1 s and the heating power was 10^5 W/m^2 (heating energy 10^4 Jm^{-2}). With such pulse duration, we may well assume that, starting from times about 0.5 s, calculated temperature histories are close to those obtained by applying Dirac-pulse heating. With time, temperature distributions are 'smashing' (Fig. 6a) but flaw sites are well seen, and the only difference between water and epoxy adhesive is in temperature amplitudes. Basic temperature profiles in Fig. 6b are identical to those in Fig. 5a, and the difference between the profiles becomes evident, for example, either in the logarithmic (Fig. 6c) or differential presentation (Fig. 6d). The calculated e_{ap} *vs.* τ profiles (Fig. 6e) are very close to the analytical ones in Fig. 5b. Note that such profiles are often shown in Log-Log coordinates, which for an adiabatic semi-infinite body, are straight lines with the slope of -0.5.

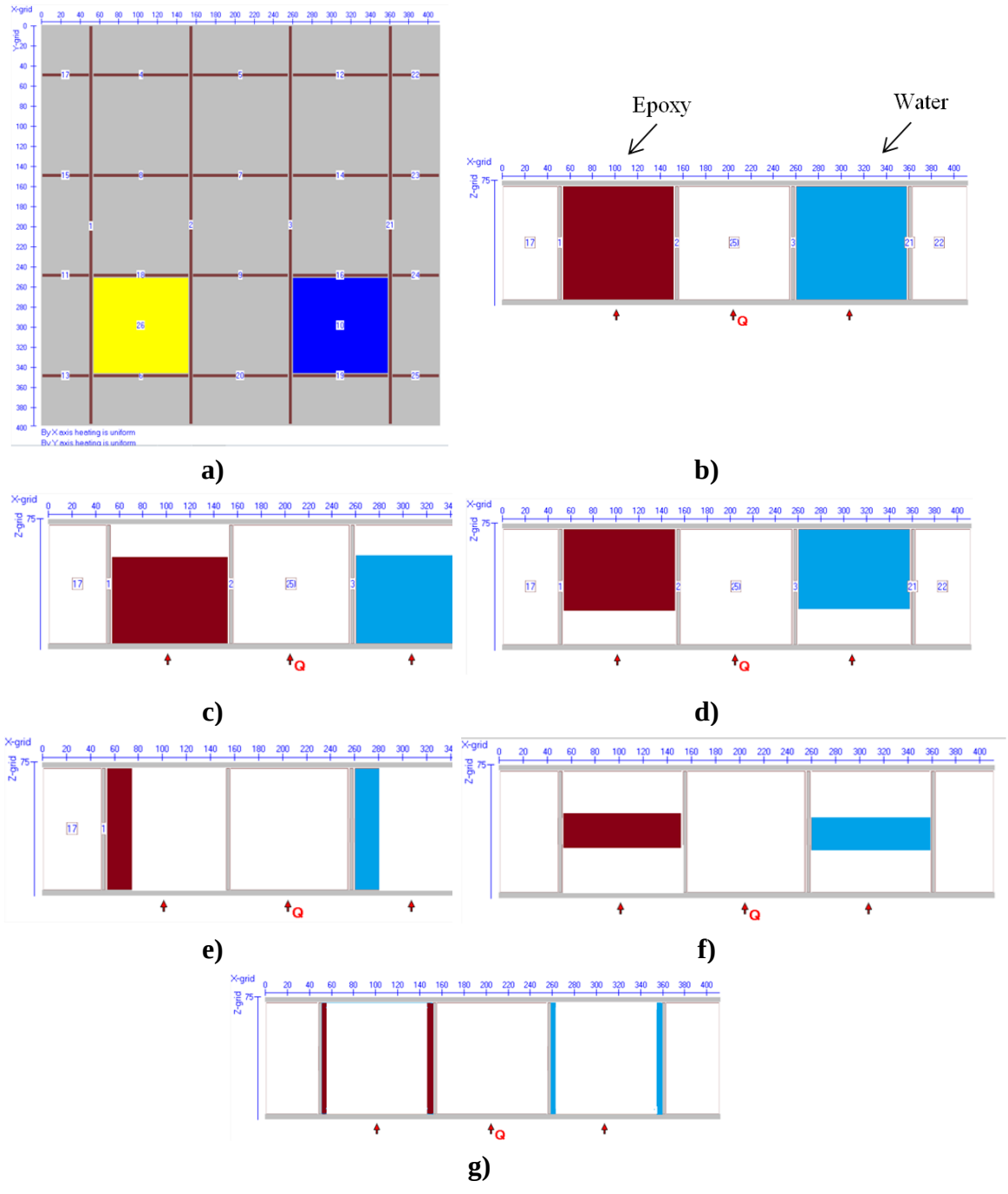

Fig. 4. 3D numerical models (ThermoCalc-3D software): a – calculation scheme (top view), b – 100 % water content, c – water down, heating from bottom, d – water down, heating from top, e – side water, side heating, f, g – capillary water.

The inflection time τ_{inf} can be considered as a time when the front surface response starts to show evidence of the back wall of a laminate or a honeycomb skin.

To find τ_{inf}, one can use two approaches. First, let us analyze the ratio $T_{SIB}(Fo)/T_P(Fo)$ between the temperatures on the surface of a semi-infinite body ('*SIB*') and a plate ('*P*') made of the same material. The corresponding plot is shown in Fig. 7.

Assume, for example, that τ_{inf} corresponds to the ratio value of 99 %, then combining Eqs. (1) and (2) yields Fo_{inf}=0.189. Another approach involves the analysis of Eq. (3). Assuming G= -1, that means full reflection of heat energy from a boundary, we obtain the same value of Fo_{inf} as above. For other G values involved, the corresponding Fo_{inf} are: 0.190 (CFRP-air), 0.223 (CFRP-epoxy) and 0.325 (CFRP-water). Hence, when developing a candidate identification algorithm, the analysis of e_{ap} should start from Fo_{inf}~ 0.2; for example, in the case of a 0.5 mm-thick CFRP skin, τ_{inf} =0.22 s.

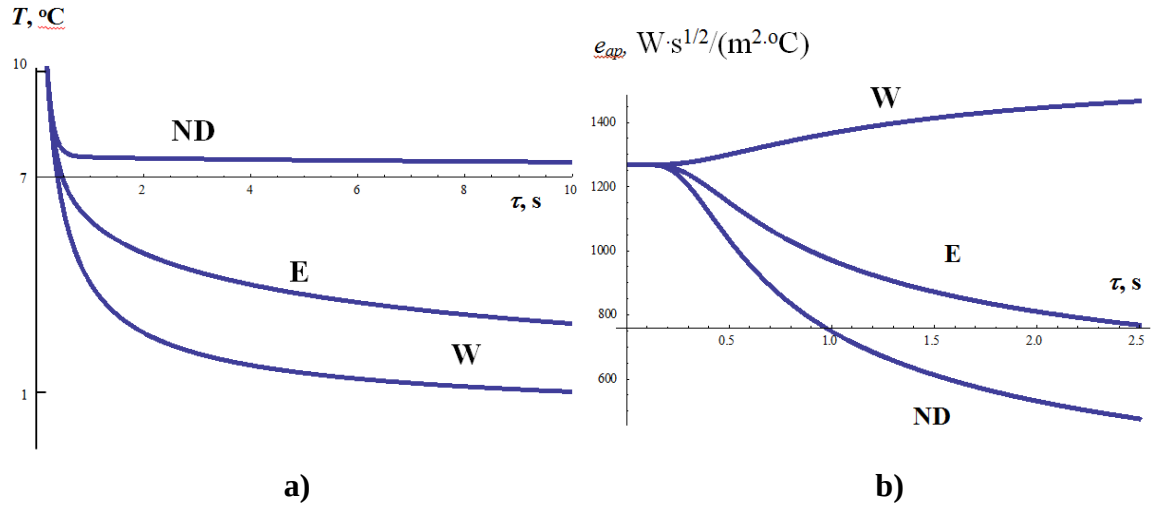

Fig. 5. 1D analytical model of water/epoxy detection by Eq. (3) (W-water, E-epoxy adhesive, ND-non-defect area): a – *T vs.* τ, b - e_{ap} *vs.* τ.

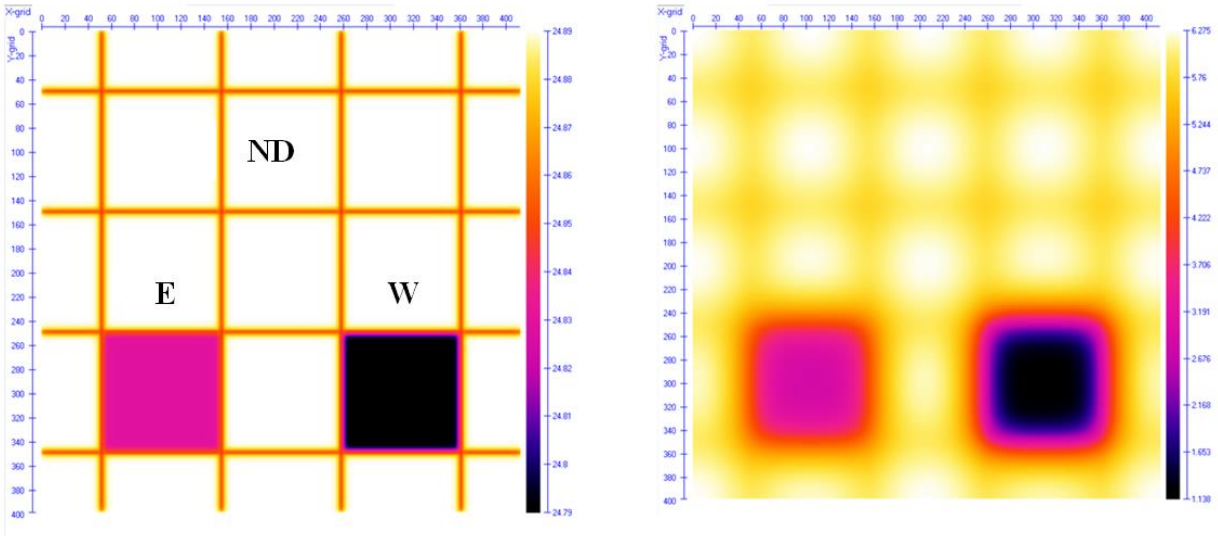
ND
E
W

a)

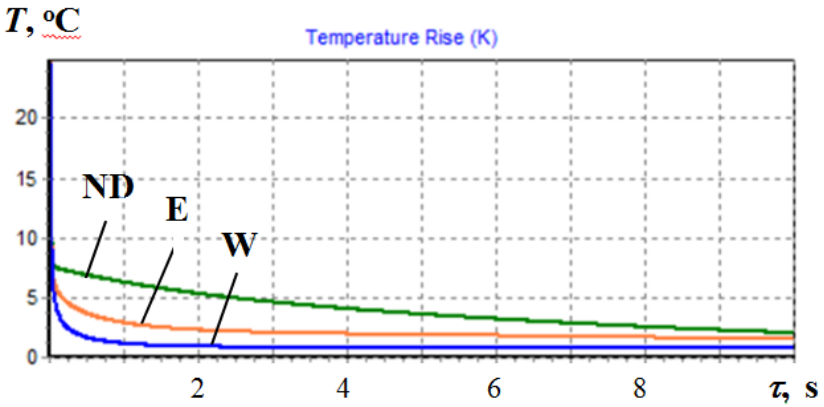
T, ºC
Temperature Rise (K)
ND
E
W
τ, s

b)

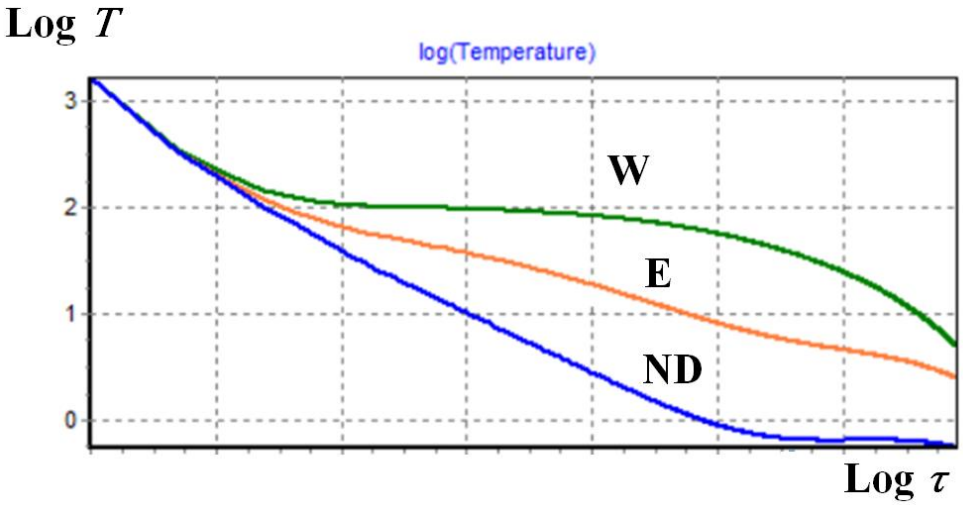
Log T
log(Temperature)
W
E
ND
Log τ

c)

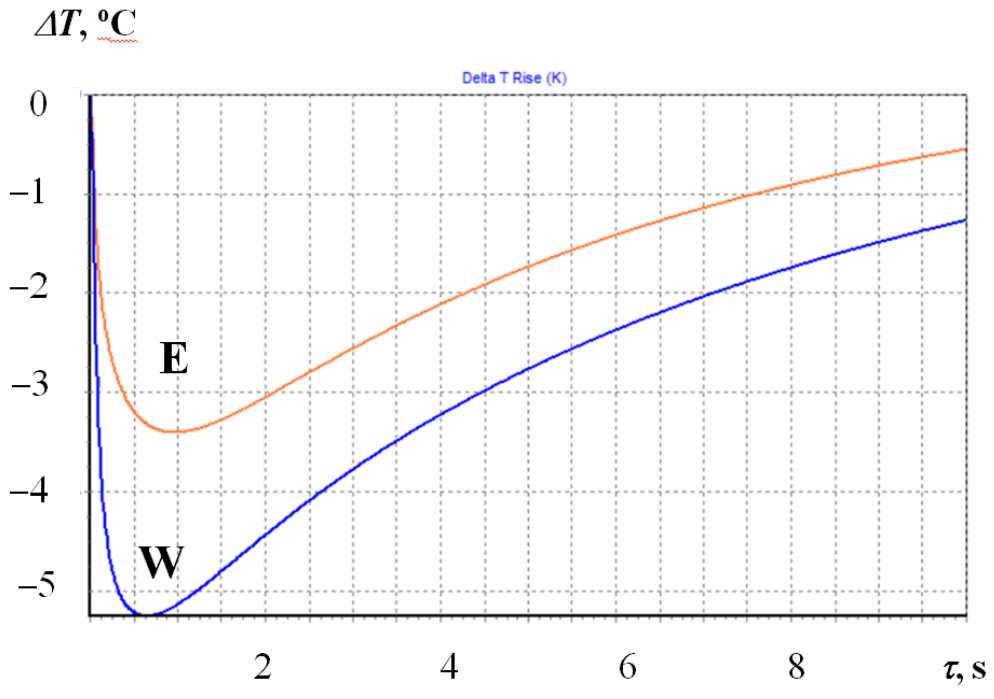

d)

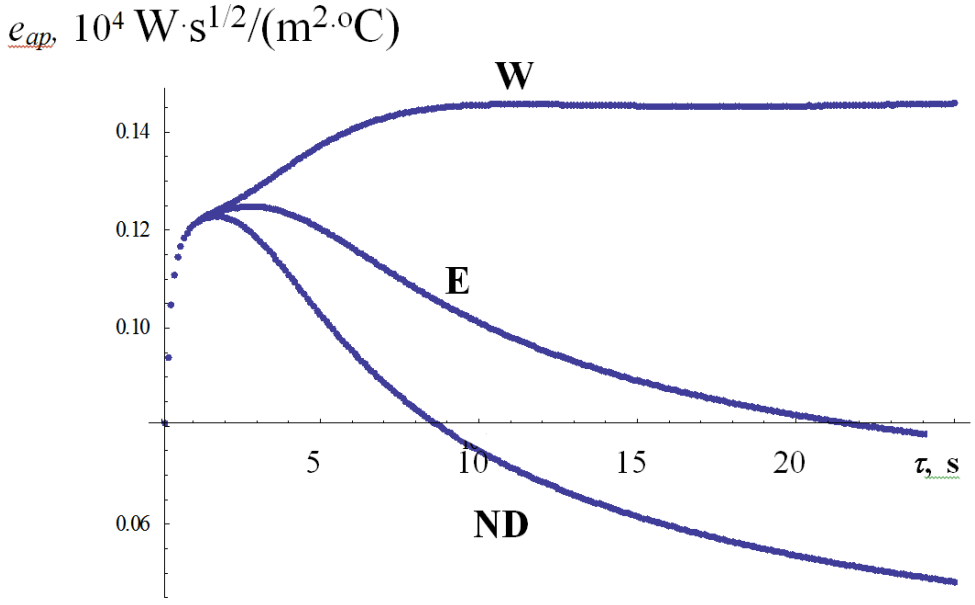

e)

Fig. 6. Analyzing 3D model in Fig. 4 (Q=10^5 W/m^2, τ_h=0.1 s, water/epoxy content 100%): a - surface temperature distributions at 0.1 s (left) and 10 s (right), b – temperature profiles (left: T *vs.* τ, middle: Log T *vs.* Log τ, right: ΔT *vs.* τ), c – Log T *vs.* Log τ, d – ΔT *vs.* τ, c – e_{ap} *vs.* τ.

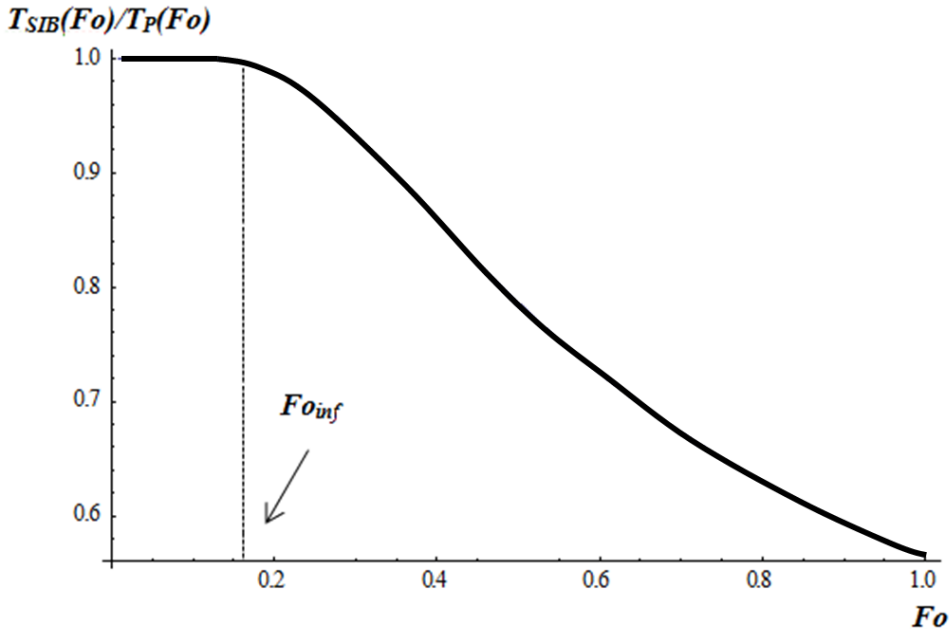

Fig. 7. $T_{SIB}(Fo)/T_P(Fo)$ *vs. Fo.*

3.2.2. Skin material and thickness

Since temperature contrasts over trapped water are predominantly determined by water/air thermal properties, it is expected that they should be weakly dependent on skin thermal parameters. This fact is confirmed with the results presented in Fig. 8 for CFRP- and GFRP-made skin of varying thickness. Below, except the differential temperature signal ΔT and its respective observation time $\tau(\Delta T)$, we will be dealing with the running contrast $C(\tau)= \Delta T(\tau)/T(\tau)$ and the respective observation time $\tau(C)$, It follows from Fig. 8a that, while skin thickness increases from 0.1 to 2 mm, the value of the maximum contrast C_m drops by 40%, while optimum observation time $\tau(C_m)$ linearly grows up, and the ratio between its values for CFRP and GFRP is approximately proportional to the ratio between the diffusivities of these materials.

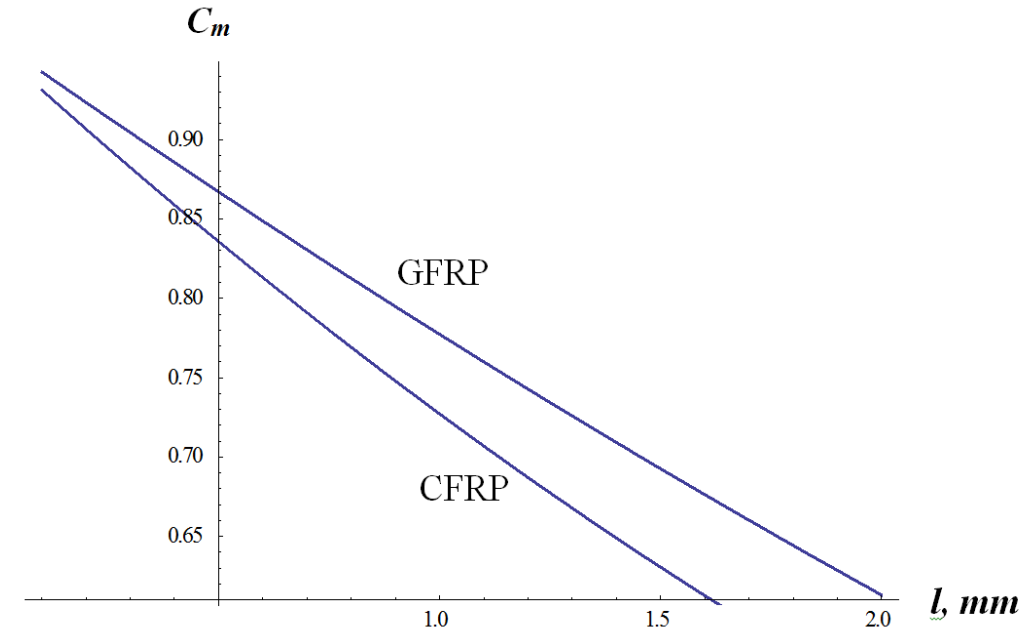

a)

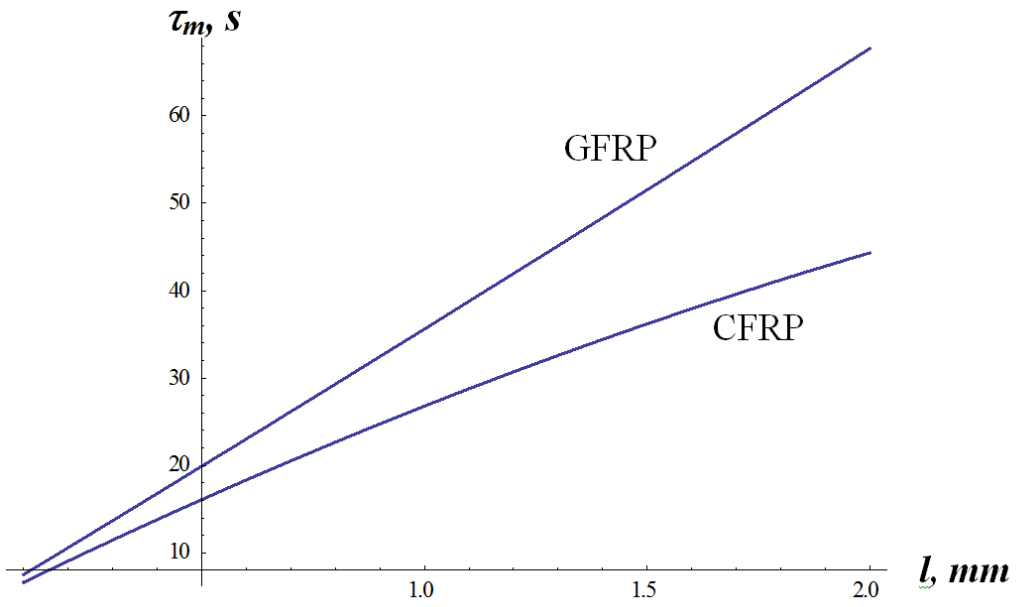

b)

Fig. 8. Temperature contrast C_m (a) and best observation time τ_m (b) vs. skin thickness l (model from Fig. 4, flash heating, water 100%)

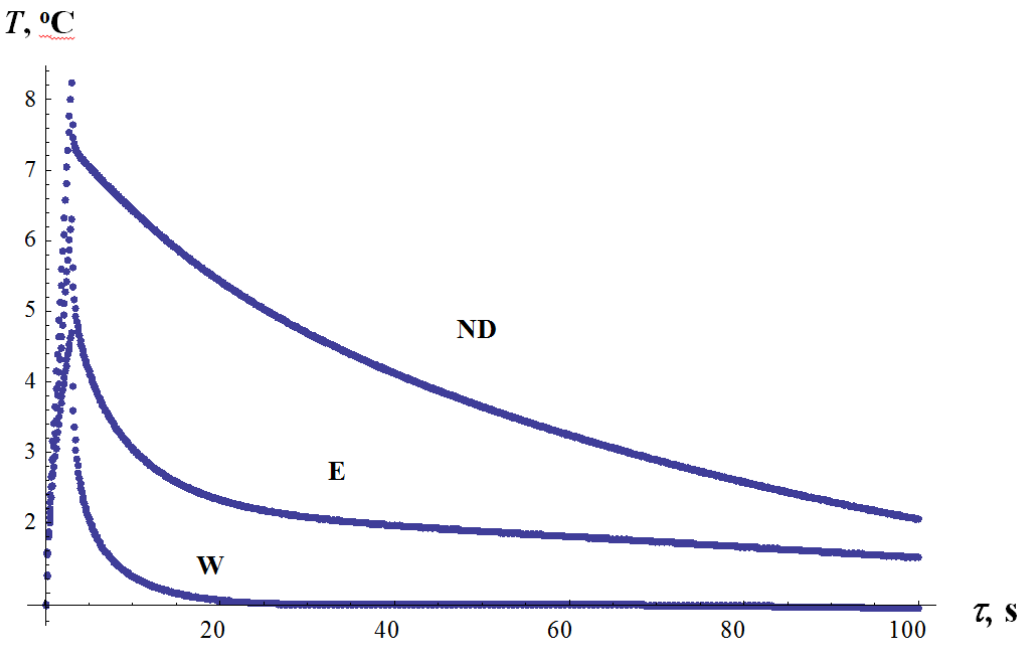

a)

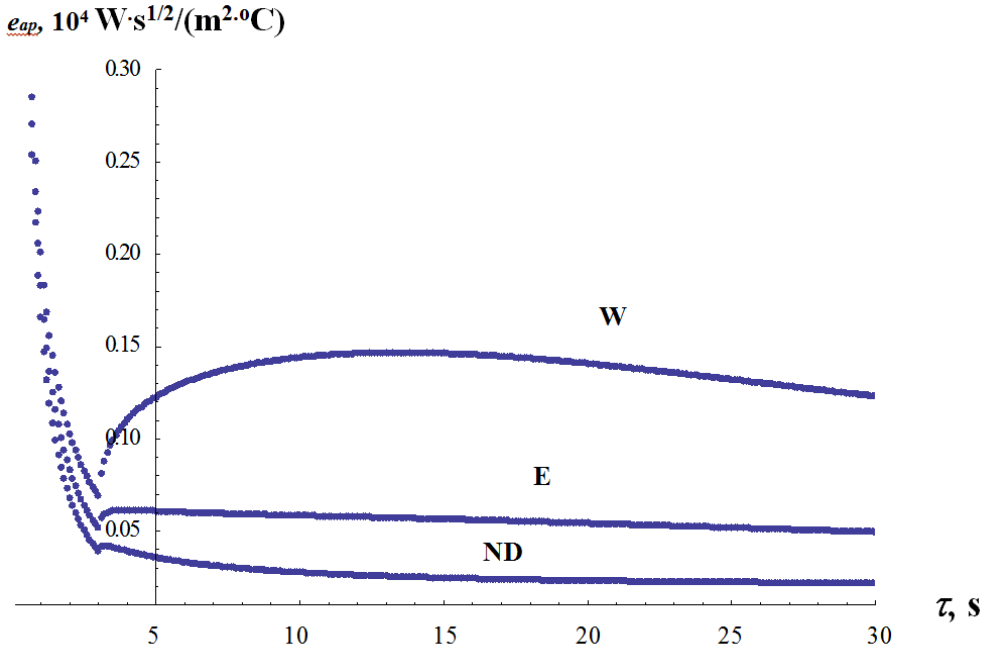

b)

Fig. 9. Analyzing 3D model in Fig. 4 in the case of square pulse heating (Q=3333 W/m^2, τ_h=3 s, W-water, E-epoxy adhesive, ND-non-defect area, water/epoxy content 100%): a - surface temperature evolutions, b – e_{ap} *vs.* τ

3.2.3. Heat pulse duration

Temperature evolutions presented in Fig. 6b for the case of flash heating, are shown in Fig. 9 for square pulse heating (τ_h= 3 s, pulse energy 10^4 Jm^{-2}). Obviously, these evolutions are very different for $\tau < \tau_h$ but they tend to acquire the same values of temperature and effusivity at longer times. Below we will see that the values of differential temperature signals and dimensionless contrasts are close while using flash and square-pulse heating.

3.2.4. Water mass evaluation

A simple quantitative estimate of water ingress in honeycomb panels can be obtained by determining the total volume of cells containing water, e.g. by multiplying the visible cell area occupied with water by the known panel thickness. Such an estimate cannot be accurate because of varying panel thickness and, particularly, because of the fact that honeycomb cells could be only partially filled with water being subjected to gravitational and capillary forces (Fig. 4).

It is anticipated that temperature, both absolute and differential, cannot characterize water content because purely amplitude characteristics are affected by many poorly-controlled parameters. As mentioned above, in this study, we analyze differential temperature signals ΔT and dimensionless contrasts signals $C=\Delta T/T$. The modeling results are presented in Table 2 and Fig. 10. Both ΔT and C evolutions are fairly classical and reveal extrema at the corresponding observation times $\tau(\Delta T_m)$ and $\tau(C_m)$. Note that the negative signs of ΔT and C mean that flaw areas, i.e. cells filled with water and/or epoxy, are colder than the surrounding (Fig. 10a). It is seen from the Table 2 that, when detecting the water which is in contact with an inspected skin, the running contrast C_m decays by 12.7 % if the water content decreases from 100 to 10%. Respectively, in the case of epoxy, C_m decays by 23 %. It is worth reminding that the C_m parameter is preferable because it is independent of absorbed heat power. But even more sensitive is the change of $\tau(C_m)$: about 62 %. Side water can be effectively detected if water mass is big enough (Fig. 10c). The explanation to the facts above is still related to the water high heat capacity.

The more difficult situation is when the water is separated from an inspected skin by an air gap (rear surface water, Fig. 10b). The air acts as a damping medium that significantly reduces both the thermal differential signal/contrast and prolongs their observation time. The absence of several $\tau(C_m)$ values in Table 1 is explained by the fact that the corresponding temperature extrema appear at later times when the absolute temperature signals ΔT become negligible.

The above-mentioned phenomena also affect the detection of water in the hypothetic cases of capillary water, although in these cases the surface temperature patterns may help water identification, as shown in Fig. 10d.

So far, modeling results using an algorithm to evaluate water content are not very encouraging. This aspect needs further development.

Table 2. 3D modeling results (models in Fig. 4)

Defect (cell volume)	Water		Epoxy adhesive	
	ΔT_m, °C (τ_m, s)	C_m (τ_m, s)	ΔT_m, °C (τ_m, s)	C_m (τ_m, s)
Cell filling 100 % (τ_h=0.1 s)				
100%	-5.26 (6.4)	-0.836 (17.7)	-3.41 (9.6)	-0.574 (19.0)
Cell filling 100 % (τ_h=3 s)				
100%	-5.24 (8.0)	-0.832 (18.7)	-3.39 (11.1)	-0.573 (20.5)
Partial cell filling, front surface water (τ_h=0.1 s)				
50%	-5.25 (6.4)	-0.835 (17.7)	-3.40 (9.6)	-0.573 (18.9)
25%	-5.25 (6.4)	-0.826 (14.3)	-3.39 (9.3)	-0.560 (15.5)
10%	-4.98 (4.5)	-0.730 (6.6)	-2.96 (5.5)	-0.442 (7.2)
5%	-4.21 (2.9)	-0.593 (3.7)	-2.18 (3.0)	-0.307 (3.7)
Partial cell filling, rear surface water (τ_h=0.1 s)				
50%	-0.438 (63.4)	-0.215 (192)	-0.295 (50.3)	-0.099 (92.7)
25%	-0.148 (51)	-*	-0.103 (38)	-
10%	-0.0474 (64)	-	-0.0313 (59)	-
5%	-0.0223 (67)	-	-0.0149 (62)	-

Partial cell filling, water in cell center (τ_h=0.1 s)				
10%	-0.440 (46.4)	-0.133 (70.2)	0.271 (33.6)	-0.663 (45.9)
Side water (τ_h=0.1 s)				
10%	-3.25 (3.8)	-0.474 (7.2)	-1.64 (3.9)	-0.238 (6.0)
Capillary water (τ_h=0.1 s)				
0.3 mm-thick layers	-1.279 (5.4)	-0.216 (20.1)	-0.938 (3.0)	-0.133 (4.5)

* Negative running contrast grows up in time while differential temperature signals tend to zero

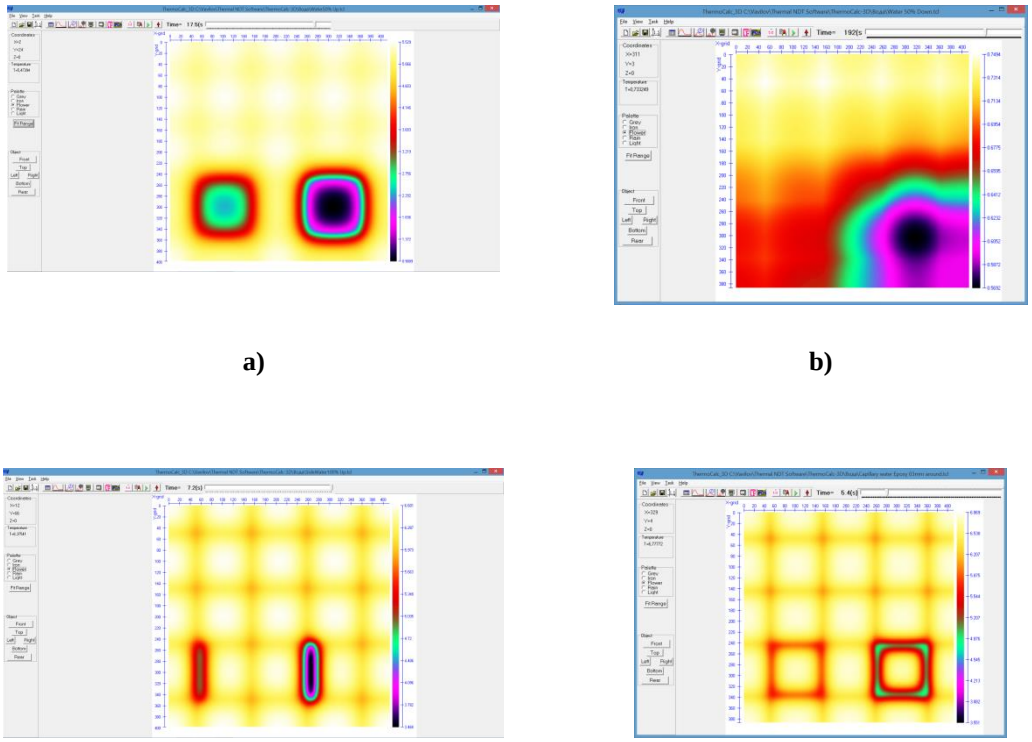

a) **b)**

c) **d)**

Fig. 10. Temperature distributions in some test cases (ThermoCalc-3D software): a – water content 50% (front surface water), observation time 17.7 s, b –50% (rear surface water), 192 s, c – 10% (side water), 7.2 s, d – water layer thikness 0.3 mm (capillary water), 5.4 s

4. Experimental results

Experimental results have been obtained on both reference and real honeycomb samples. In order to avoid phenomena of capillary water which may be present in small-size cells, the reference sample represented 4 large-size cells (Fig. 11a). Inspection was

performed on both surfaces to understand how water content affects the surface temperature indications. The detection reliability was evaluated by the signal-to-noise ratio for the cell B in regard to the cell A: $S=\Delta T/\sigma_{nd}$, where σ_{nd} is the temperature standard deviation in a non-defect area.

In the case of raw images, the cells fully and partially filled with water can be hardly discriminated. Also, the *S* value drops down by the order of magnitude if water is separated from the inspected skin by an air gap. The corresponding IR image sequences have been processed by applying some algorithms that are well known in TNDT [8, 9]. The achieved *S* values show that no single algorithm can provide optimum results in all test cases. For example, to better detect thin layers of water, the wavelet analysis seems to be the best (S=58.1 to compare to 12.3 in the source image, Fig. 11b). While inspecting the rear surface (Fig. 11c), the highest S=2.3 appears by applying the technique of autocorrelation; however, in this case, neither of processing algorithms provides essential improvement of *S* to compare to the source image.

The next sample was an aviation honeycomb panel (0.5 mm-thick glass fiber skin, 12 mm-high Nomex paper cells) which contained two 20×20 mm areas filled with water and epoxy glue by 100 %.

In the raw image at the optimum observation time (τ=5 s), the ‘defect’ areas differed only by the surface temperature (Fig. 12a) while the evolution of effusivity exhibited anomalous behavior in sites that contained water (Fig. 12b) similar to that in Fig. 5b. The binary map in Fig. 12b shows the water site distinctly. This image includes only pixels where the apparent effusivity begins to increase after the inflection time, which is about 0.3 s, as seen in Fig. 12b.

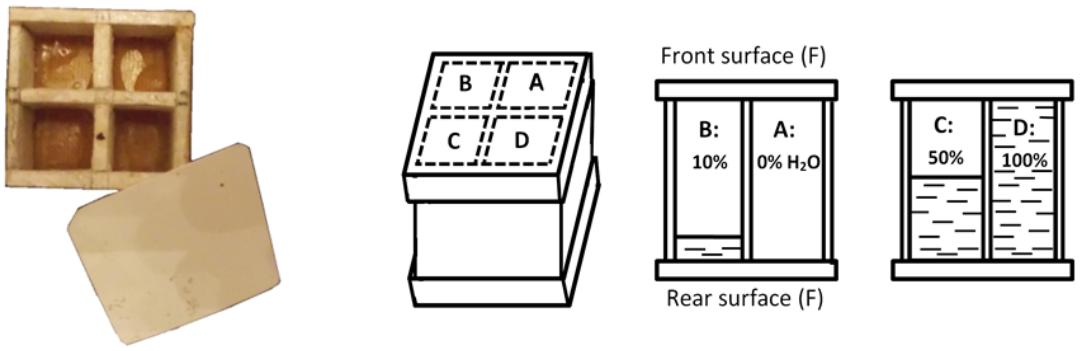

a)

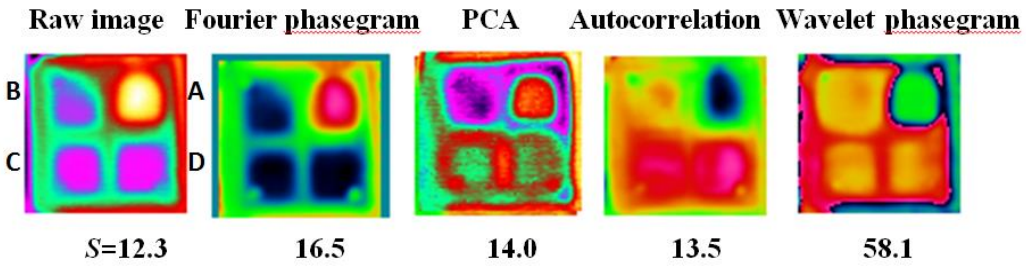

b)

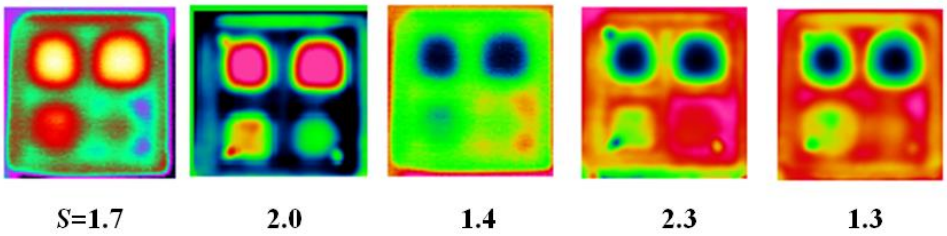

c)

Fig. 11. "Standard" data processing in active TNDT of hidden water in a honeycomb reference sample (0.5 mm plastic skin, 20×20×23 mm cell, 500 W halogen lamp, 10 s heating stage, 20 s cooling stage): a - scheme of defects, b - one-sided test on front surface, c - one-sided test on rear surface (*S* values are given for cell B in regard to cell A).

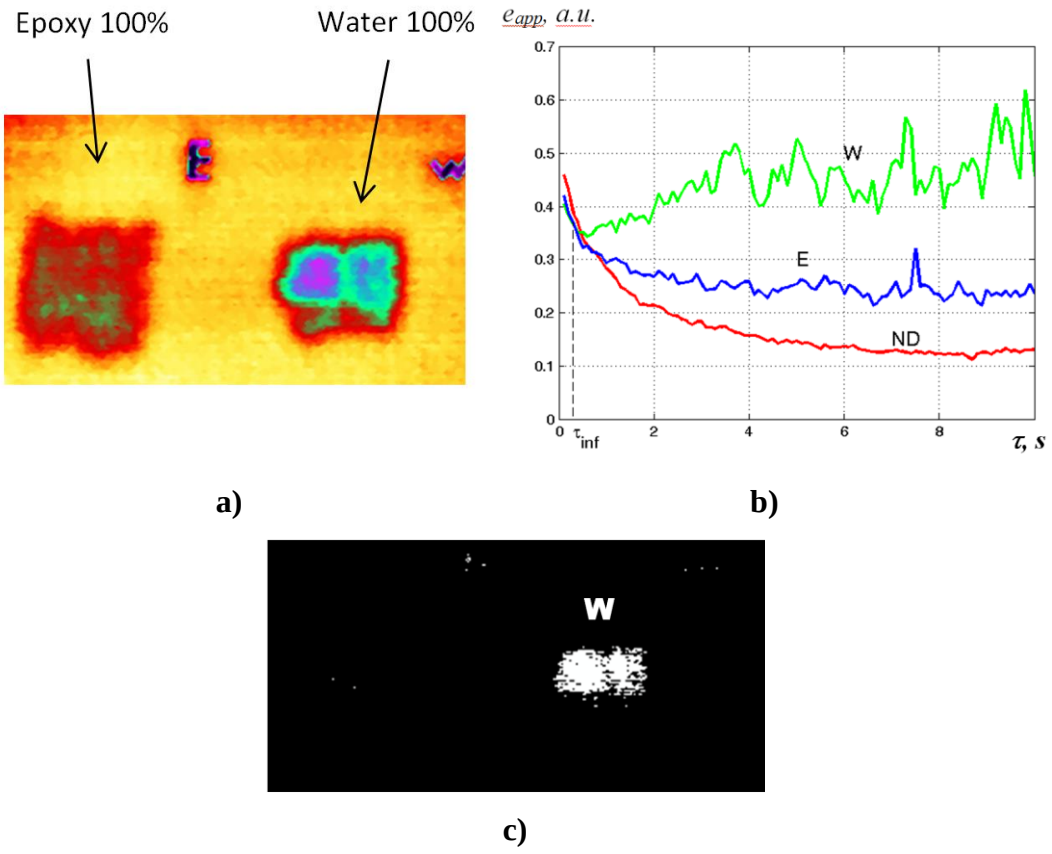

Fig. 12. Discriminating between water and epoxy in an aviation honeycomb panel (0.8 mm-thick glass fiber skin, 10 mm-high Nomex paper cells, two 20×20 mm defect areas): a - best source image (τ=5 s),b – e_{ap} *vs.* τ,c – binary map (processing effusivity map at τ=7 s, τ_{inf} ~0.3 s).

Finally, the concept of apparent effusivity has been validated on another honeycomb sample (0.5 mm-thick glass fiber skin, 12 mm-high Nomex cells) where 5 defects contained different fillings (3 areas with water and 2 areas with epoxy adhesive, see Fig. 13). On the front surface where both water and epoxy contacted the skin, all 5 defects were clearly detected after heating the sample for 3 s (Fig. 13a, b). The analysis of apparent effusivity resulted in the binary map shown in Fig. 13c where only water-filled cells were underlined. It is worth noting that the very similar image was obtained by applying principle component analysis (PCA) but this processing algorithm lacks a physical meaning, and its results are not so predictable as in the case of effusivity analysis. Much worse were results obtained on the sample rear surface. Defect detection was possible in this case

(Fig. 14a,b) but the effusivity binary map, as expected, revealed only the defect 5 with 100% water (Fig. 14c) where the apparent effusivity increased by over 10 % to compare to early time values.

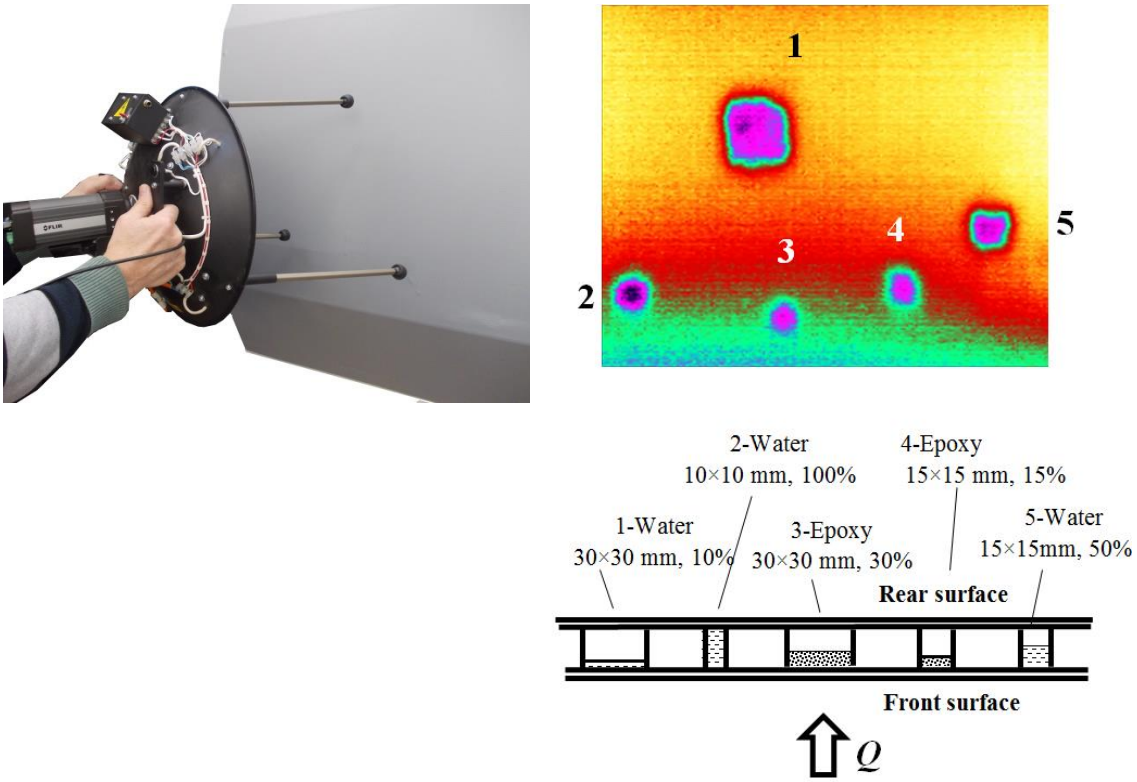

Fig. 13. Detecting water and epoxy adhesive in aviation honeycomb panel (0.5 mm-thick glass fiber skin, 12 mm-high Nomex cells, five defect areas water in contact with skin): a – inspecting aviation honeycomb panel (TNDT inspection unit, Tomsk Polytechnic University), b – defect scheme and 'best' source image at 4.6 s (optimum for detecting defect 5), c – binary map (processing effusivity map at τ=4 s, τ_{inf} ~0.3 s), d – 2nd component (PCA technique)

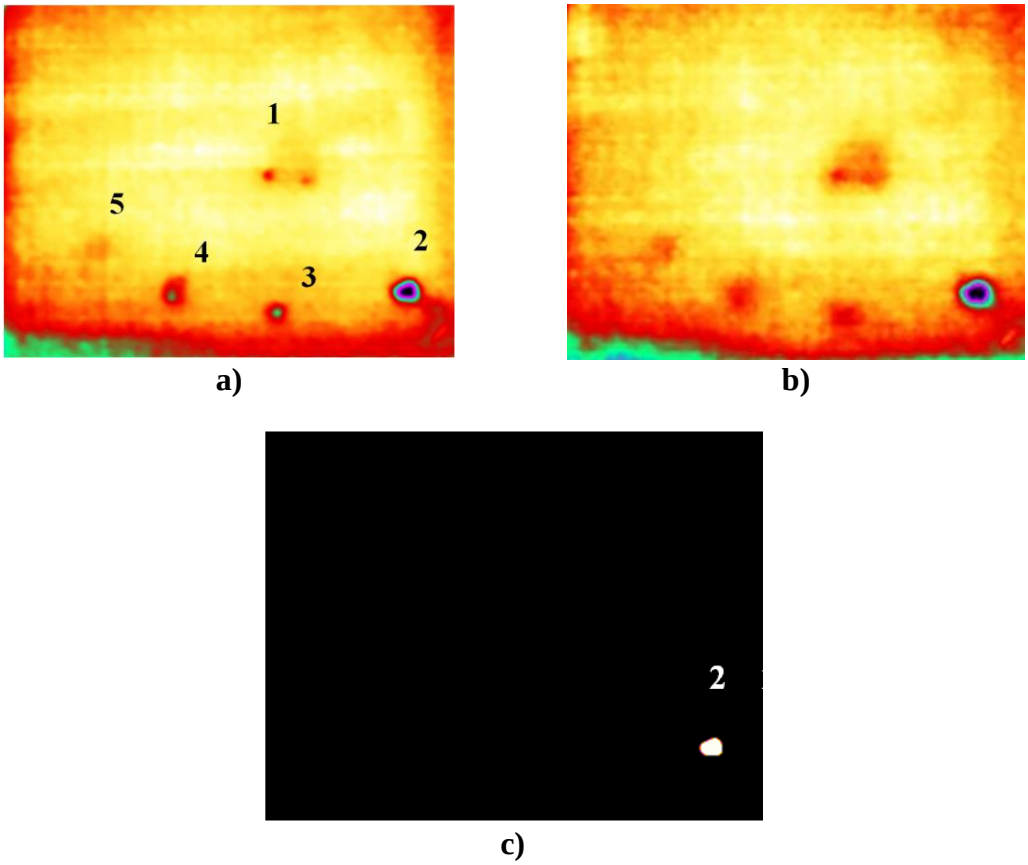

Fig. 14. Detecting water and epoxy adhesive in an aviation honeycomb panel (0.5 mm-thick glass fiber skin, 10 mm-high Nomex cells, five defect areas, air gaps between water and skin): a – 'best' source image at 21.6 s (optimum for detecting defect 5),
b – effusivity distribution at 21.6 s, c – binary map (processing effusivity map at τ=4 s, τ_{inf} ~0.3 s)

4. Conclusions

- 1D and 3D models of water detection in aviation honeycomb panels were analyzed with an emphasis on the evaluation of water mass and the ability to discriminate between water and epoxy adhesive.
- The surface temperature signals are highest if water contacts the skin of a honeycomb panel. In this case, discrimination can be made only between a thin layer of water and fully-filled cells. Therefore, it is very difficult to establish a reliable relationship between a mass of water and a corresponding temperature signal by using the approach documented in this study. If the trapped water is not in contact with the skin, but is separated from it by a small air gap, the temperature signal is reduced by an order of magnitude and the corresponding observation times become longer.

- The surface temperature contrasts over trapped water are determined predominantly by the thermal properties of water and air and they are only weakly dependent on the thermal properties and thickness of the composite skin.
- Using a classical active thermal NDT test, it is difficult to discriminate between water and epoxy adhesive by analyzing only the surface temperature patterns. The concept of apparent effusivity has demonstrated both theoretically and experimentally, that the cell-water can be reliably detected by an increase in effusivity starting from the inflection time. Alternately, the effusivity decays over honeycomb cells filled with air and epoxy adhesive.
- In future research, tests will be conducted on real aircraft panels. A data processing algorithm will be developed to estimate the water mass.

This research was supported in part by NIR #445(ONG), State order of the Russian Ministry of Higher Education for 2 014-2016, and by National Natural Science Foundation of China (No. 61571028).

References

1. H. Kersemans, I. De Baere, J. Degrieck, K. Van Den Abeele, L. Pyl, F. Zastavnik, H. Sol, W. Van Paepegem. Nondestructive damage assessment in fiber reinforced composites with the pulsed ultrasonic polar scan. Polym Test 2014; 34: 85.

2. NDT Handbook on Infrared technology, ASNT Handbook Series, X. Maldague technical, P.O. Moore (eds.). American Society for Nondestructive Testing Press (2001): 718.

3. V. Vavilov, A. Klimov. D. Nesteruk. Detecting water in aviation honeycomb structures by using transient IR thermographic NDT. Proceedings of SPIE "Thermosense-XXV" 2003; 5073: 345.

4. V.P. Vavilov, D.A. Nesteruk. Detecting water in aviation honeycomb structures: the quantitative approach. Quant. Infra Red Thermography J. 2004; 1(2): 173.

5. C. Ibarra-Castanedo, F. Marcotte, M. Genest, L. Brault, V. Farley, X.P.V. Maldague. Detection and characterization of water ingress in honeycomb structures by passive and active thermography using a high resolution camera. Proceedings of 11th Intern. Conf. Quant. IR Thermography, Naples, Italy 11-14 June 2012: 10.

6. A318/A319/A320/A321 Nondestructive Testing Manual, Part 10 A, 55-20-06-Thermographic, Page block 1001.
7. Boeing 777 Nondestructive Testing Manual, Part 9-Thermography.
8. Guo Xingwang. V.P. Vavilov. Pulsed thermographic evaluation of disbonds in the insulation of solid rocket motors made of elastomers. Polym Test 2015; 45: 31.
9. V. Vavilov, Dynamic thermal tomography: perspective field of thermal NDT. Proceedings of SPIE "Thermosense-XII" 1990; 1313: 178.